High-Voltage and High-Safety Practical Lithium Batteries with Ethylene Carbonate-Free Electrolyte

Yu Wu,[1] Dongsheng Ren,[1,2] Xiang Liu,[1,3] Gui-Liang Xu,[3] Xuning Feng,[1,*] Yuejiu Zheng,[4] Yalun Li,[1] Min Yang,[1] Yong Peng,[1] Xuebing Han,[1] Li Wang,[2,*] Zonghai Chen,[3] Yang Ren,[5] Languang Lu,[1] Xiangming He,[2] Jitao Chen,[6] Khalil Amine,[3,7,8,*] and Minggao Ouyang[1,*]

[1] State Key Laboratory of Automotive Safety and Energy, Tsinghua University, Beijing 100084, China.
[2] Institute of Nuclear and New Energy Technology, Tsinghua University, Beijing 100084, China.
[3] Chemical Sciences and Engineering Division, Argonne National Laboratory, Lemont, IL 60439, United States.
[4] College of Mechanical Engineering, University of Shanghai for Science and Technology, Shanghai 200093, China
[5] X-ray Science Division, Advanced Photon Source, Argonne National Laboratory, Lemont, IL 60439, United States.
[6] Beijing National Laboratory for Molecular Sciences, College of Chemistry and Molecular Engineering, Peking University, Beijing 100871, China.
[7] Materials Science and Engineering, Stanford University, Stanford, CA 94305, United States.
[8] Institute for Research& Medical Consultations (IRMC), Imam Abdulrahman Bin Faisal University (IAU), Dammam, Saudi Arabia.

* Corresponding authors:
fxn17@mail.tsinghua.edu.cn;
wang-l@mail.tsinghua.edu.cn;
amine@anl.gov;
ouymg@mail.tsinghua.edu.cn

Abstract

Serious safety issues are impeding the widespread adoption of high-energy lithium-ion batteries for the transportation electrification and large-scale grid storage. Herein, we report a triple-salt ethylene carbonate (EC)-free electrolyte for high-safety and high-energy pouch-type $LiNi_{0.8}Mn_{0.1}Co_{0.1}O_2$|graphite (NMC811|Gr) cells. This EC-free electrolyte can effectively stabilize NMC811 surface under high potential (up to 4.5 V), as well as generate stable interphase to achieve a superior compatibility with the Gr anode. The electrolyte strategy enables significantly enhanced intrinsic safety (trigger temperature of thermal runaway increased by 67.0 °C), excellent

electrochemical properties (4.2V, ~100 % after 200 cycles), and superior high voltage stability (4.5 V, 82.1 % after 200 cycles). The work opens up a new avenue for developing novel electrolyte systems to build safer high-energy batteries for practical applications.

Introduction

With the ambitious target of being carbon neutral, high-performance energy storage devices for transportation electrification and large-scale grid storage are highly desirable.[1,2] Among the various energy storage devices, lithium ion batteries (LIBs) have been world-widely adopted owing to relative high specific energy/power and long cycle life.[3] To further increase the specific energy, researchers are pushing the chemical limits of LIBs,[4-9] which leads to more serious battery safety issues hindering the further commercialization of large-scale applications.[10,11]

The severe safety concern, generally presented as thermal runaway (TR), is triggered by the poor thermal tolerance of aggressive Ni-rich cathodes at charged state, especially when it encounters highly reductive ethylene carbonate (EC).[12,13] Tremendous efforts are made to address safety concerns, including optimization of separator[14,15], cathode[8,16], current collector[17], and the use of non-flammable electrolyte[18-21]. Although such efforts can somewhat reduce the risk of TR, more efforts are urgently required to obtain intrinsically safe LIBs for practical applications. The traditional $LiPF_6$/EC-based electrolytes have dominated the electrolyte market for more than 25 years,[22] but they are hard to cope with new battery chemistry,[23,24] and strongly questioned for their high flammability. In this regard, the design of 'safe' electrolytes with simple, effective, and low-cost features is important for the next-generation batteries.

As EC solvent contributes greatly to both surface parasitic reactions causing performance fading and initial self-heating before TR, as well as exothermic reactions triggering battery TR, building "EC-free" electrolytes is the most convenient and efficient strategy to improve the intrinsic safety. Moreover, the low cost, low viscosity, and environmentally friendly EC-free electrolytes have recently been demonstrated to

operate well in LIBs.[25-28] Unfortunately, the research stops short of safety performance of cells with EC-free electrolyte. Moreover, the electrochemical performance of EC-free electrolyte in practical Ah-level full cells needs to be investigated urgently.

Meanwhile, the construction of robust electrode-electrolyte interface (EEI) has been regarded as a fascinating strategy to relieve these above-mentioned safety concerns and enhance the electrochemical properties.[29-36] The robust EEI can significantly mitigate the release of oxygen, and suppress the interfacial side reactions. Moreover, the formation approach is perfectly compatible with the current battery technology for industrial manufacture. Inspired by these prominent advantages, the combination of EC-free electrolyte and robust EEI skin is extremely attractive.

In this work, we report high-safety of 10 Ah pouch-type $LiNi_{0.8}Mn_{0.1}Co_{0.1}O_2$|graphite (NMC811|Gr) batteries with EC-free electrolyte based on the exclusively aprotic acyclic carbonate solvents. By adopting triple-salt, the EC-free electrolyte (0.8 M LiFSI-0.1 M LiTFSI-0.6 M $LiPF_6$/ EMC) can effectively stabilize NMC811 surface under high working potential, as well as generate stable interface to achieve a good compatibility with the Gr anode. The combined strategy resulted in excellent electrochemical properties (~100 % capacity retention after 200 cycles), significantly enhanced intrinsic thermal characteristics (TR trigger temperature increased by 67.0 ºC), and extended cell-to-cell TR propagation time within module (average TR propagation time is doubled). Even under the harsh conditions of high working potential of 4.5 V, the practical NMC811|Gr pouch cells can still retain 82.1 % of their original capacity after 200 cycles, which is 8 times higher than the retention of conventional EC-based electrolyte. The work opens up a whole new direction for both tailoring the electrode materials and developing practical technologies for safe LIBs.

Results and discussion

Electrochemical performance of practical pouch-type NMC811|Gr full cells

The ionic conductivity of varied electrolytes with different lithium salt

concentration are summarized in Table S1, Supporting Information. The electrochemical performance of ~200 mAh NMC811|Gr batteries with varied electrolytes at 1 C rate is presented in Figure S1, Supporting Information. When only the EC is removed without changing the salt species and concentration (1.0 M $LiPF_6$/ EMC), the pouch cell exhibits the worst ionic conductivity (4.38 mS cm^{-1}) and cycling performance (~4.0 % after 100 cycles). By simply changing the species of single $LiPF_6$ salt to triple salts (LiFSI/LiTFSI/$LiPF_6$), conductivity (4.75 mS cm^{-1}) and cycling performance can be improved slightly. Based on the above-mentioned results, when increasing LiFSI salt content to further improve conductivity (6.44 mS cm^{-1}), the pouch cell with EC-free electrolyte exhibits optimal cycle performances (~89 % after 100 cycles) and average coulombic efficiency (~100.0%), which are far superior to those of conventional EC-based electrolyte (capacity retention: ~75% after 100 cycles; coulombic efficiency: 99.3%) and triple-salt EC-based electrolyte at same salt concentration (capacity retention: ~77% after 100 cycles; coulombic efficiency: 99.6%). In addition, the rate performance of EC-free electrolyte is not inferior to that of conventional EC-based electrolyte (Figure S2, Supporting Information).

The cycling stability and high-voltage stability of NMC811|Gr batteries were presented in Figure 1. The excellent cyclability of batteries with EC-free electrolyte is confirmed by the overlapped charge/discharge curves (Figure 1a) and ~ 100% capacity retention after 200 cycles (Figure 1b). Under the harsh high voltage condition, the electrochemical performances were further evaluated. Through improving the working potential from 4.2 V to 4.5 V, the capacity can be increased from 959.8 mAh to 1155.4 mAh (Figure 1a-d).

As shown in Figure 1e, the capacity of NMC811/Gr full cell in EC-based electrolyte drops quickly over 140 cycles. Meanwhile, the obvious fluctuation of CE over 140 cycles is observed, implying the severely interfacial side reactions in the EC-based electrolyte. However, the opposite phenomenon is observed for the EC-free electrolyte. The superior high-voltage stability (4.5 V, 82.1 % after 200 cycles) and high CE (>99.9%) for the full cell with EC-free electrolyte verify the formation of robust EEI on NMC811 cathode and Gr anode, which prevents the electrolyte

consumption during charging and discharging cycling.

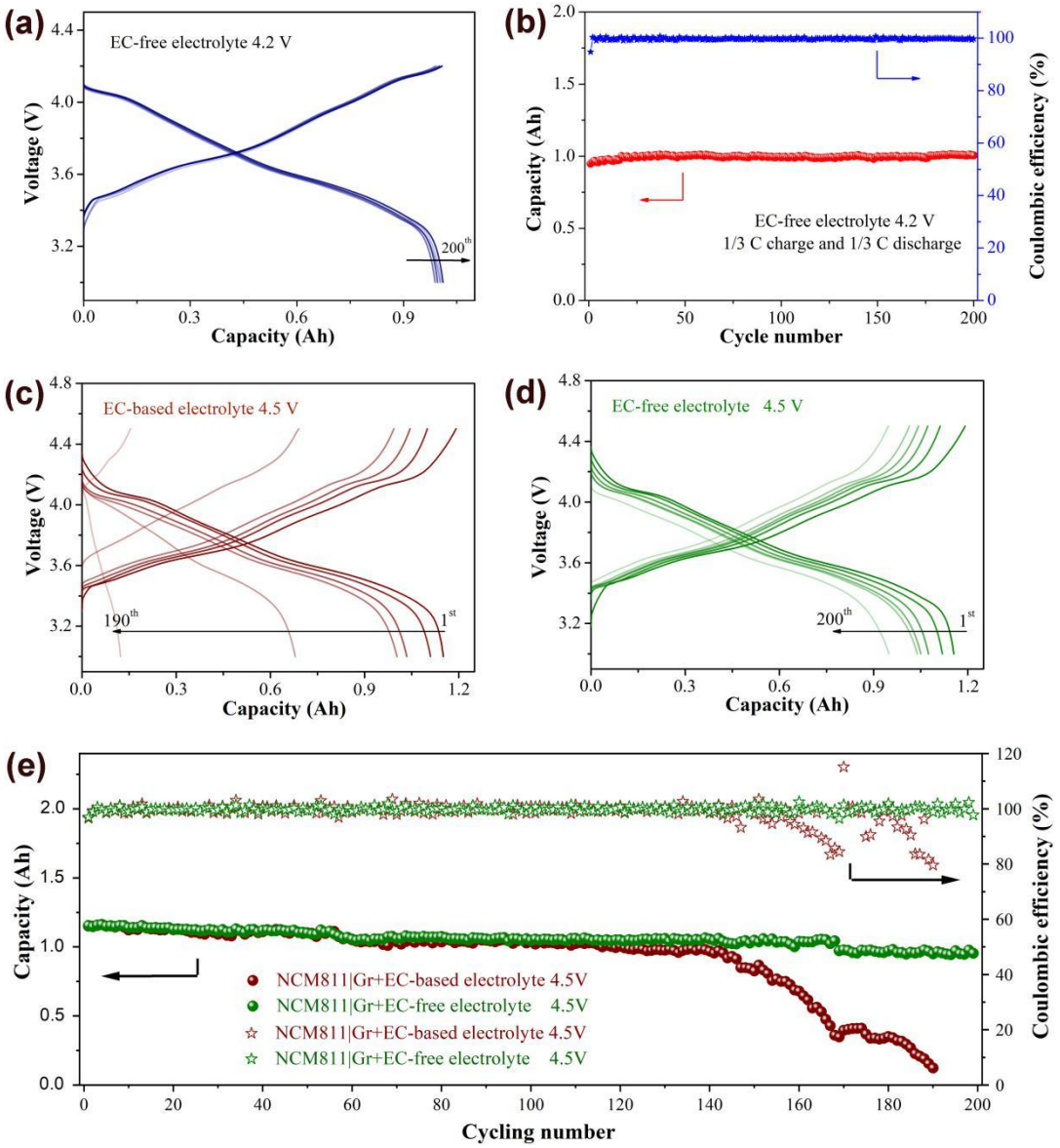

Figure 1. Electrochemical Behavior of NMC811|Gr batteries. (a) Charge-discharge curves of NMC811|Gr using EC-free electrolyte cycled at 4.2 V. (b) Cycling stability of NMC811|Gr using EC-free electrolyte when cycled at 1/3 C. (c,d) Charge-discharge curves of NMC811|Gr using EC-based and EC-free electrolyte cycled at 4.5 V, respectively. (e) Cycling stability of NMC811|Gr using EC-based and EC-free electrolyte cycled at 4.5 V.

Safety performance of practical pouch-type NMC811|Gr full cells

The accelerating rate calorimetry (ARC) was adopted to investigate the safety features of 10 Ah NMC811|Gr practical batteries with EC-based and EC-free

electrolytes.[37-39] For the battery with EC-based electrolyte (Figure 2a,b), T_2 is only located at 193.1 °C, resulted from the severe side reactions between the reactive NMC811 and the conventional EC-based electrolyte. Surprisingly, T_2 of the battery with EC-free electrolyte reaches 260.1 °C and simultaneously with OCV falling (Figure 2c,d), which is 67.0 °C higher than that of the above-mentioned battery. To the best of our knowledge, the TR trigger temperature T_2 (260.1 °C) is the highest value obtained that have been reported for the high-energy NMC811-based cells via all kinds of safety improvements, including advanced fire-extinguishing concentrated electrolyte (195.2 °C).[13,40,41] Moreover, the intrinsic safety performance of NMC811-based cell with EC-free electrolyte can even far exceed the level of improved NMC523-based cell with ceramic polyethylene terephthalate non-woven separator (231 °C).[12]

Nail penetration and overcharge test were conducted to further judge the practical safety of the pouch cell. During the nail penetration process (Figure S3, Supporting Information), the highest temperature of 1 Ah battery with EC-free electrolyte is only 520.0 °C, which is much lower than that of battery with EC-based electrolyte (637.0 °C). It is worth noting that, when the nail is inserted, the EC-based electrolyte cell immediately catches fire and quickly reaches the highest temperature. However, the temperature of EC-free electrolyte cell rises slowly, and the time to reach the highest temperature can be effectively delayed by 250s. Neither of the two electrolyte pouch cells caught fire or exploded during the overcharge test. After overcharge test, the temperature of the cell with EC-based electrolyte higher than that of the EC-free electrolyte cell (Figure S4, Supporting Information). These results demonstrate that the EC-free electrolyte could improve the intrinsic safety of cells, which is attributed mainly to the removal of the trigger reactions between EC and NMC811.

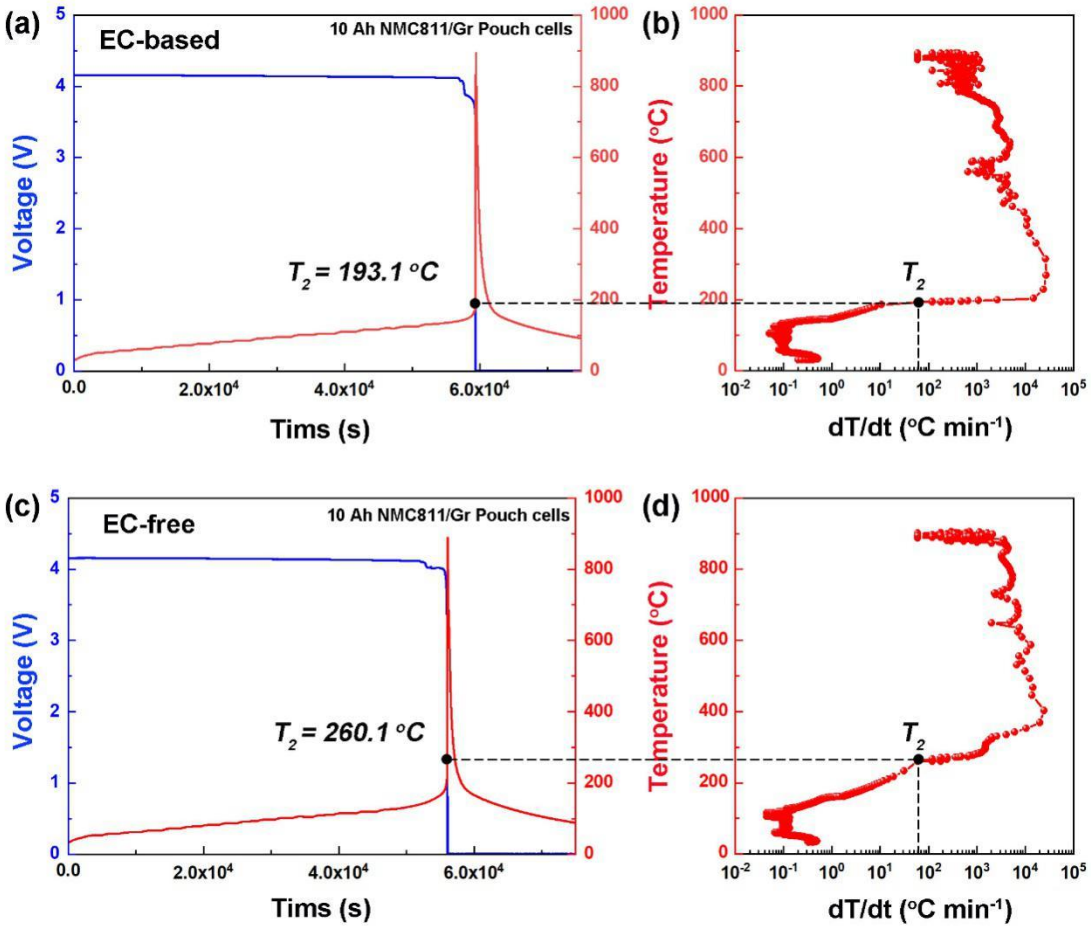

Figure 2. Safety features of 10 Ah NMC811|Gr batteries. (a,b) Batteries with the EC-based electrolyte. (c,d) Batteries with the novel EC-free electrolyte.

Figure 3 shows the temperature profiles and three-dimensional distributions of the 9-cell module during TR propagation simulation. The TR propagation time of EC-based electrolyte with T_2 = 193.1 °C yields 5.25 s from cell x to x+1, and the 9-cell TR within 189 s (Figure 3a). However, the EC-free electrolyte with high T_2 value (260.1 °C) can significantly extend the average TR propagation time to cell i/i+1 =9.88 s, and the 9-cell TR at 278 s (Figure 3b). As shown in Figure 3c, the TR propagation time sequence map of the modeling analysis clearly present that the TR in cell1 with EC-base electrolyte is triggered at 145 s. Surprisingly, while all 9 cells with EC-based electrolyte are triggered into TR, the first cell1 with EC-free electrolyte has not yet been triggered. Effective suppression of cell-to-cell TR propagation within module, resulted from the enhanced intrinsic safety of the single

cell by removing EC solvent.

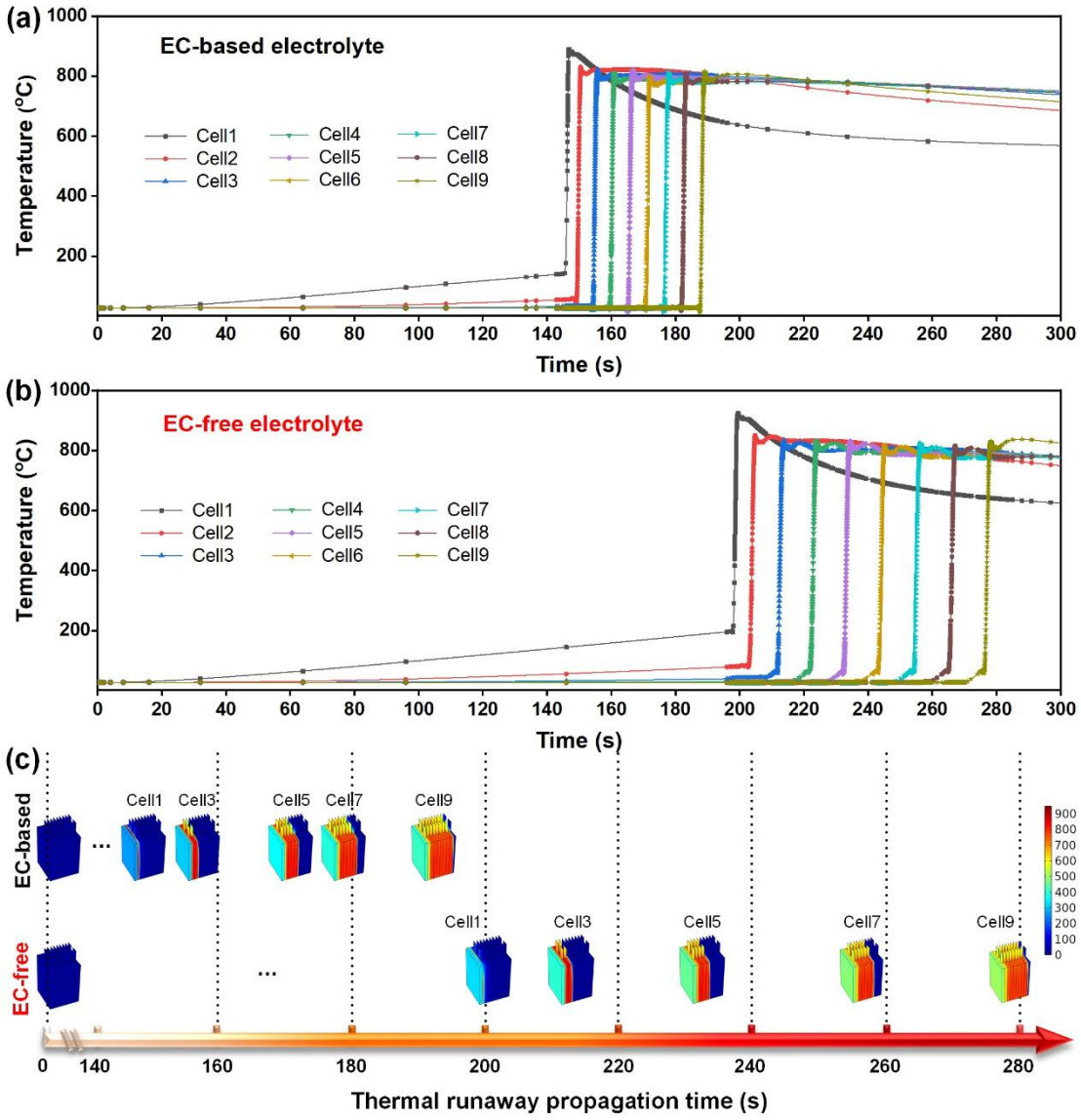

Figure 3. Thermal runaway propagation simulation of the 9-cell module in Comsol Multiphysics®. (a,b) The temperature profile of cells calculated in the thermal runaway propagation model for different electrolytes, respectively. (c) The thermal runaway propagation time sequence map of the modeling analysis.

Thermal stability of different electrolytes with charged NMC811

The thermal runaway of pouch-type NMC811|Gr batteries is closely related to the thermal stability of charged cathode with the presence of electrolyte.[42] In this regard, *operando* synchrotron high-energy X-ray diffraction (HEXRD) was conducted to study the thermal stability.[12] Figure 4a-c show the curves of charged cathodes with

different electrolytes from 50 ºC to 350 ºC. The (003) peaks of NMC811 cathodes weakening start at 203 and 236 ºC for the EC-based and EC-free electrolytes (Figure 4a,b), respectively. The slower phase transformation (improved by 33 ºC) clearly demonstrates that the removal of EC solvent greatly benefits the structural stability of the charged NMC811, attributed to the effective blocking of exothermic reactions oxygen and EC solvent. Moreover, the spinel (220) peak[42,43] emerges at 169 °C for charged NMC811 with EC-based electrolyte compared with 308 °C for charged NMC811 with EC-free electrolyte, demonstrating a significantly delayed phase transition process (increased by 139 °C) for the cathode with the EC-free electrolyte.

DSC test was used to further characterize the heat flow of the different electrolytes mixed with charged NMC811. As shown in Figure 4d, the extremely strong exothermic peak emerges at 201.4 °C for the charged NMC811 with EC-based electrolyte. In sharp contrast, the intensity and rate of heat flow of EC-free electrolyte can be significantly inhibited. Moreover, the heat flows of the graphite anode with the different electrolyte are summarized in Figure S5, Supporting Information. Compared with the slow heat flow (from 50 ºC to 125 ºC) of graphite with EC-free electrolyte, the conventional electrolyte presents more intense heat flow at ~100 ºC. These results demonstrate that TR reactions at the material level can be effectively suppressed in the EC-free system, which is consistent with the excellent safety performance of NMC811|Gr batteries (Figure 2 and Figure 3).

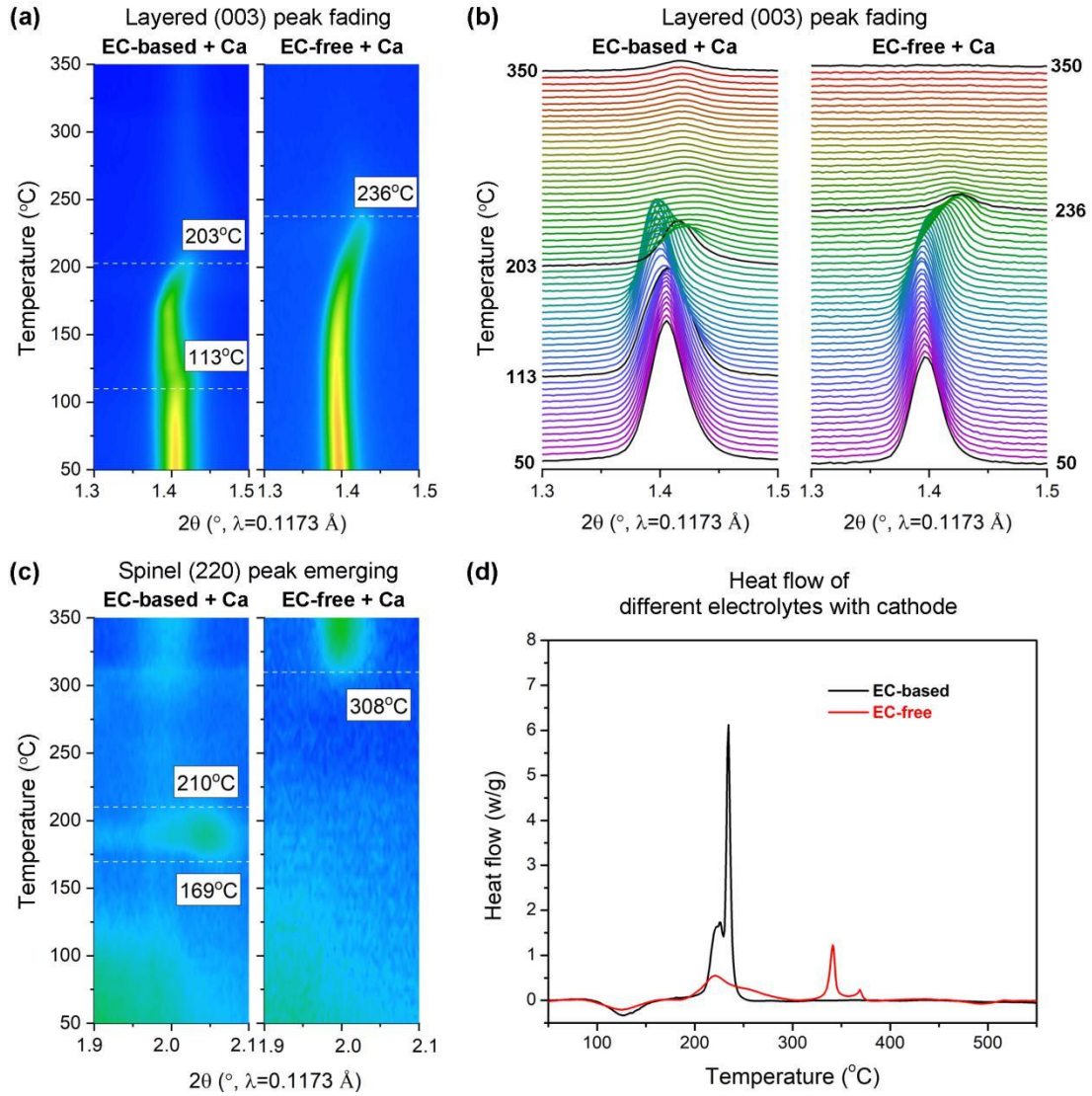

Figure 4. Thermal stability of charged NMC811 with the different electrolytes. (a,b) The contour plots and the corresponding (003) peak fading during heating of charged NMC811 with different electrolytes. (c) The contour of the (220) peak emerging during heating of charged NMC811 with different electrolytes. (d) DSC curves of the delithiated NMC811 with the presence of different electrolytes.

Characterization of the EEI on cycled electrode

In LIBs, the EEI is a significantly critical factor for the safety and electrochemical performance.[29] To confirm the generation of stable cathode-electrolyte interphase (CEI), the chemical compositions and the depth distribution of elements of the cycled cathodes were detected using XPS and FIB-SEM-ToF-SIMS combined system (Figure 5), respectively. As shown in the C 1s

spectra of XPS (Figure 5a, e), the CEI of cathodes cycled in the EC-based electrolyte contains more organic species because of the solvent decomposition, which is supported by the higher contents of C-O and C=O. In contrast, the unique feature of the CEI generated in the EC-free is more inorganic, resulted from significantly strong LiF signal (685 eV, F 1s, Figure 5b, f). In addition, the N (NO_x, 398.4 eV, N 1s, Figure 5c, g) and S (SO_4^{2-}, 169.8 eV, S 2p, Figure 5d, h) signals are only found in CEI for the EC-free electrolyte, which is derived mainly from salt anions.[44] The surface morphology and depth distribution of elements of NMC811 are presented in Figure 5i-o. Compared with the NMC811 from EC-based electrolyte, particularly high F contents are observed in the NMC811 from EC-free electrolyte (Figure 5k, n, and o). The inorganic F-rich CEI is beneficial to suppress cathode phase transformation, electrolyte decomposition, and correspondingly cathode/electrolyte parasitic reactions.

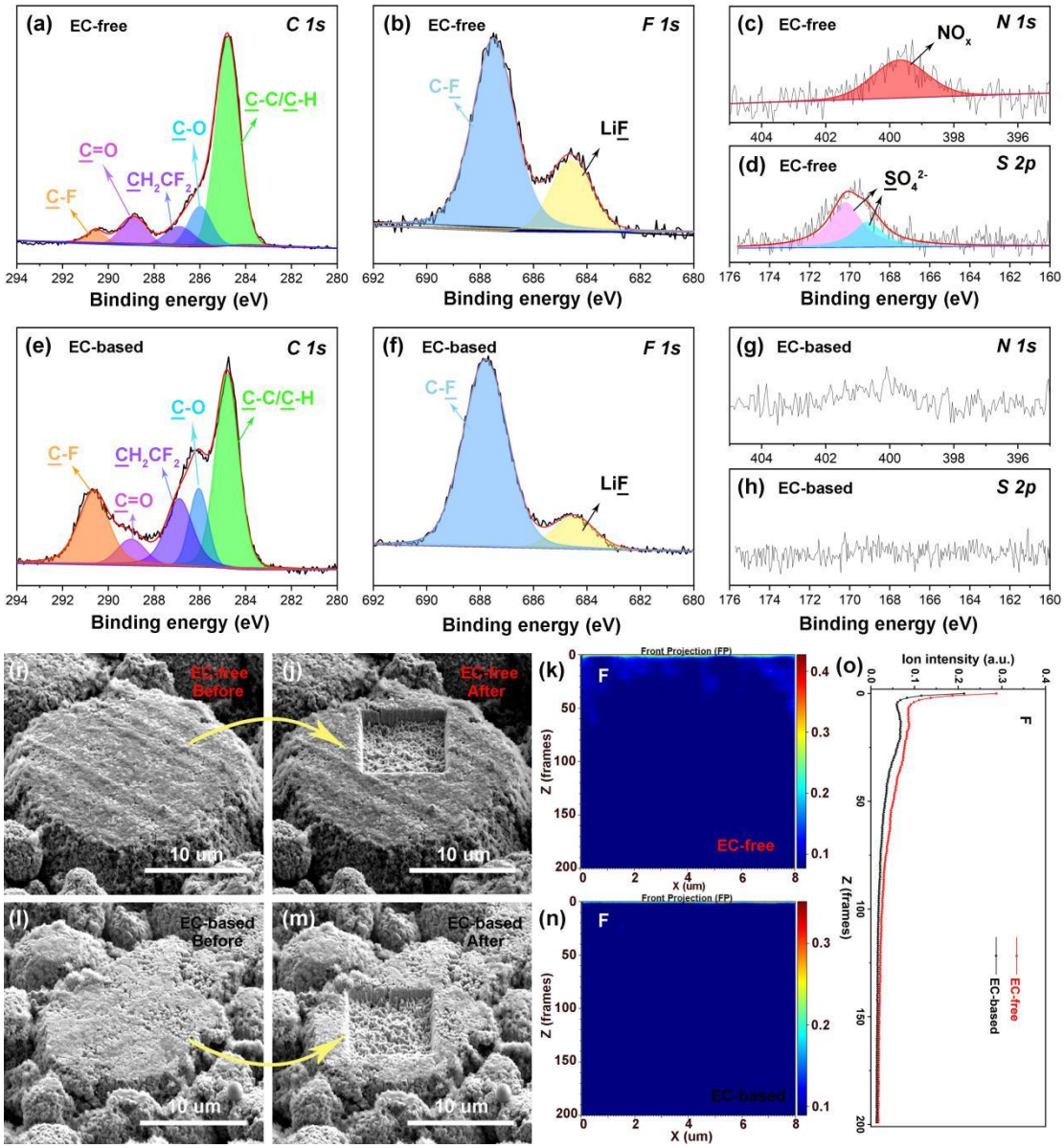

Figure 5. The CEI chemical compositions and depth distribution of the cycled NMC811. (a-h) XPS characterization of the CEI formed on NMC811 cycled using EC-free electrolytes (a-d) and EC-based electrolytes (e-h). The C 1s, F 1s, N 1s and S 2p spectra. (i-o) FIB-SEM-ToF-SIMS characterization of the NMC811 cycled using EC-free electrolytes (i-k) and EC-based electrolytes (l-n).

In order to further analyze the the CEI generated in these electrolytes, secondary-ion fragments (e.g., CH_3O^-, LiF_2^-, and PO_2^-) were detected.[45] Organic species containing CH_3O^- fragments are dwindled on the surface of cathode cycled in EC-free electrolyte (Figure 6a,b). Moreover, the high contents of LiF_2^- are achieved

(Figure 6c,d), indicating the interface of cathodes cycled in EC-free electrolyte contains more robust inorganic species. Different from EC-based electrolyte, the CEI of NMC811 in EC-free electrolyte shows weaker PO_2^- fragments signals (Figure 6e,f), attributed to the reduced content of $LiPF_6$ salt. These above-mentioned results further demonstrate that more stable inorganic compositions are formed in the surface of cathodes cycled in EC-free electrolyte.

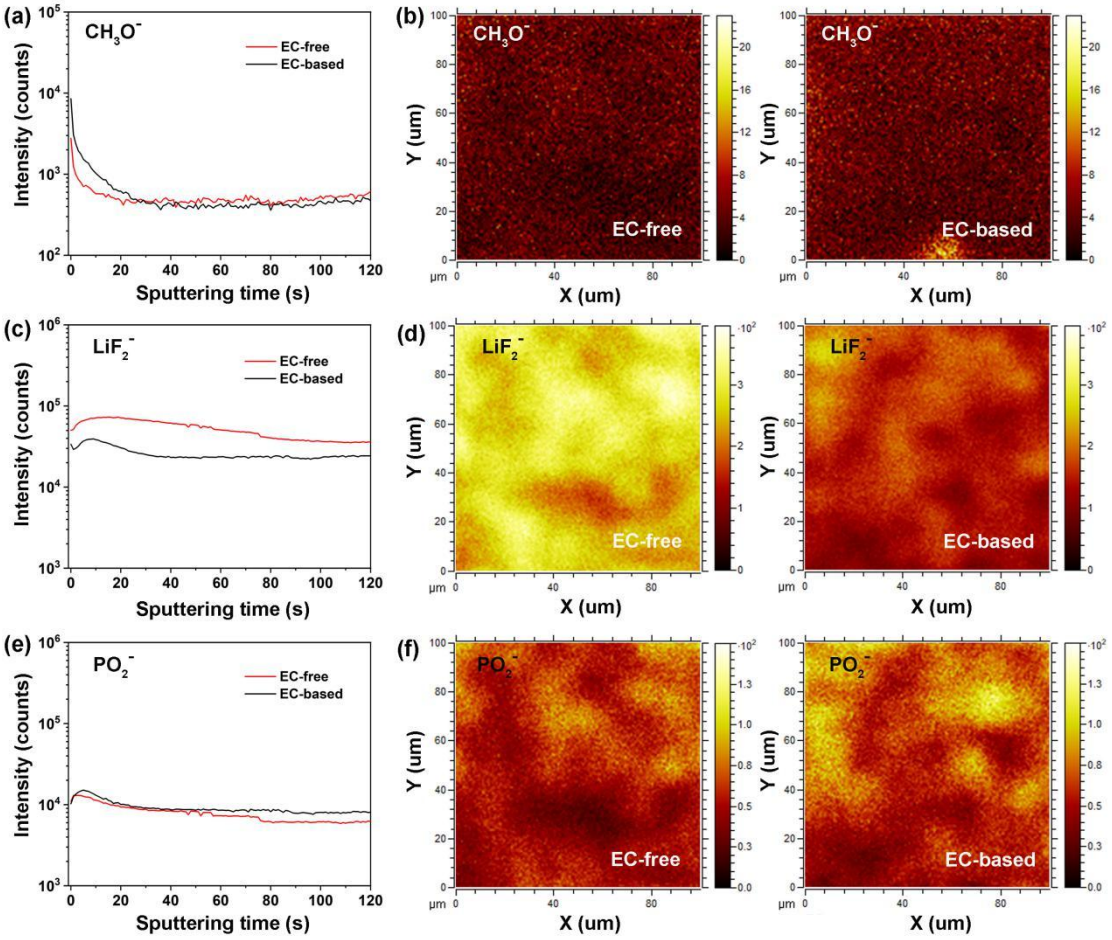

Figure 6. ToF-SIMS spectra of interfaces on the NMC811 cathodes. (a,b) Depth profiling and chemical maps of CH_3O^- on the NMC811 cathodes. (c,d) Depth profiling and chemical maps of LiF_2^- on the cycled NMC811 cathodes. (e,f) Depth profiling and chemical maps of PO_2^- on the cycled NMC811 cathodes.

Deeper insight into the NMC811 cycled in EC-free electrolyte was achieved from STEM characterization. As shown in Figure 7a-h, the mapping suggests uniform distribution of F, N, and S elements at the surface of NMC811 cycled in the EC-free

electrolytes, which are derived mainly from the salt anions FSI^-. Disordered rock-salt phase (~7.2 nm) with the thick and uneven amorphous CEI layer (~2.5 nm) are found on the NMC811 cycled in EC-based electrolyte (Figure 7i,j), suggesting the weak surface stability. In sharp contrast, significantly improved structural integrity is found in the pouch-type NMC811|Gr full cells with EC-free electrolyte. As illustrated in Figure 7k, the cycled NMC811 cathodes present a very thin cation mixing layer (~1.3 nm). Combining the performance in cycling and high-voltage, the stable inorganic CEI generated on cathodes can inhibit the interfacial side reactions (Figure 7l). These results confirm the significance of the robust and stable CEI on efficient protection of NMC811.

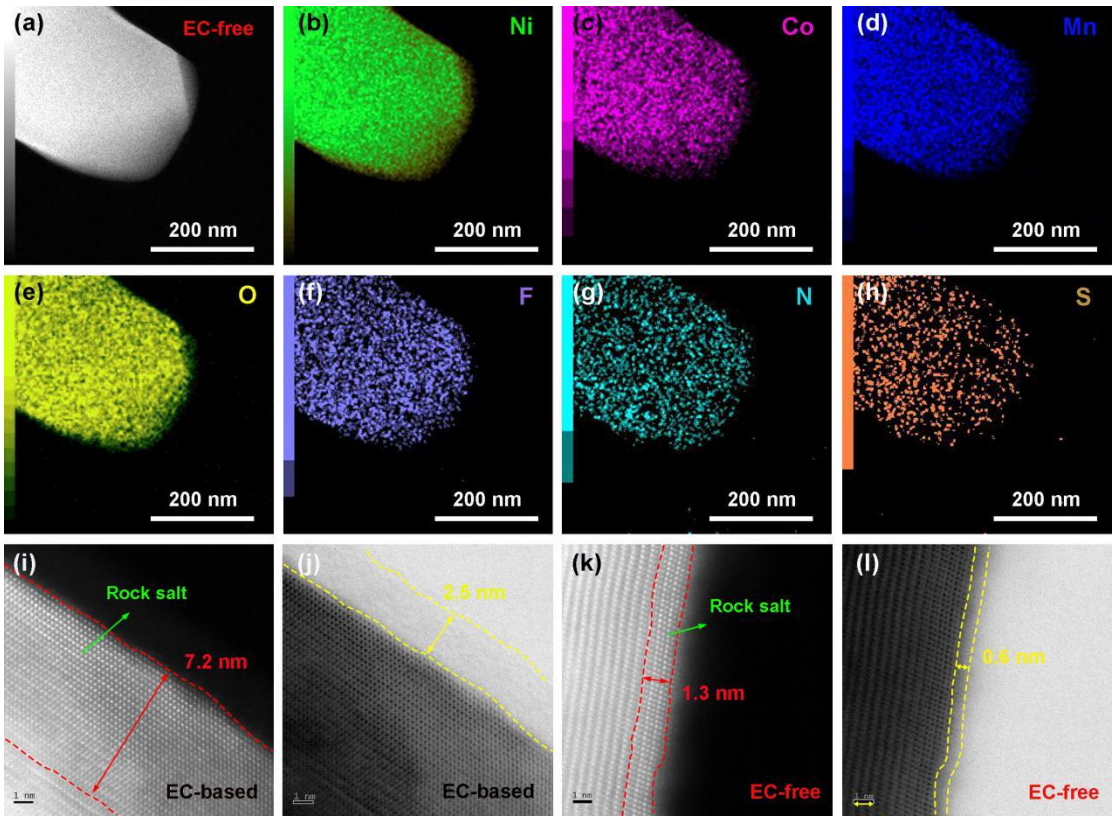

Figure 7. Structural characterization of the cycled NMC811 cathodes. (a-h) Elemental distribution in NMC811 cycled using EC-free electrolytes obtained from STEM-EDX. (i-l) STEM-HAADF and STEM-ABF images of cathodes cycled using EC-based electrolytes (i,j) and EC-free electrolytes (k,l).

In addition to the F-, N-, and S-rich CEI skin generated on the NMC811 cathodes, the solid electrolyte interphase (SEI) on the Gr anode is also a key factor. The FIB-SEM-ToF-SIMS combined system was firstly used to characterize the morphology and element depth distribution of the surface of the cycled Gr anode (Figure 8a–e). Figure 8a,b show the surface features of Gr anode before and after Xe^+ ions sputtering. After 100 cycles in EC-free electrolyte, the Gr anode maintains a clean and smooth surface (Figure 8a). When the electrolyte is changed to EC-based, a non-uniform and rough surface layer is observed (Figure 8b). Furthermore, as confirmed by the FIB-ToF-SIMS characterization of the anode shown in Figure 8c, significantly high N and S components are observed in the EC-free electrolyte. With the adoption of triple-salt ($LiPF_6$+LiFSI+LiTFSI) and the removal of EC solvent, homogeneous SEI layer is generated on the anode, containing F, N, and S species (Figure 8d,e).

XPS was employed to further analyze the chemical compositions of the SEI formed on the Gr anodes. Similar to the characterization results of CEI formed on the NMC811 cathodes, N (NO_x, 398.4 eV, N 1s, Figure 8f, h) and S (SO_4^{2-}, 169.8 eV, S 2p, Figure 8g, i) are only found in SEI for the EC-free electrolyte. These XPS analysis data of SEI layer coincide well with the above-mentioned FIB-SEM-ToF-SIMS results. Considering the superior cyclability of practical batteries in EC-free electrolyte (Figure 1), we can conclude that the F-, N, and S-rich SEI has the similar or even better effect than the SEI derived from traditional electrolyte.

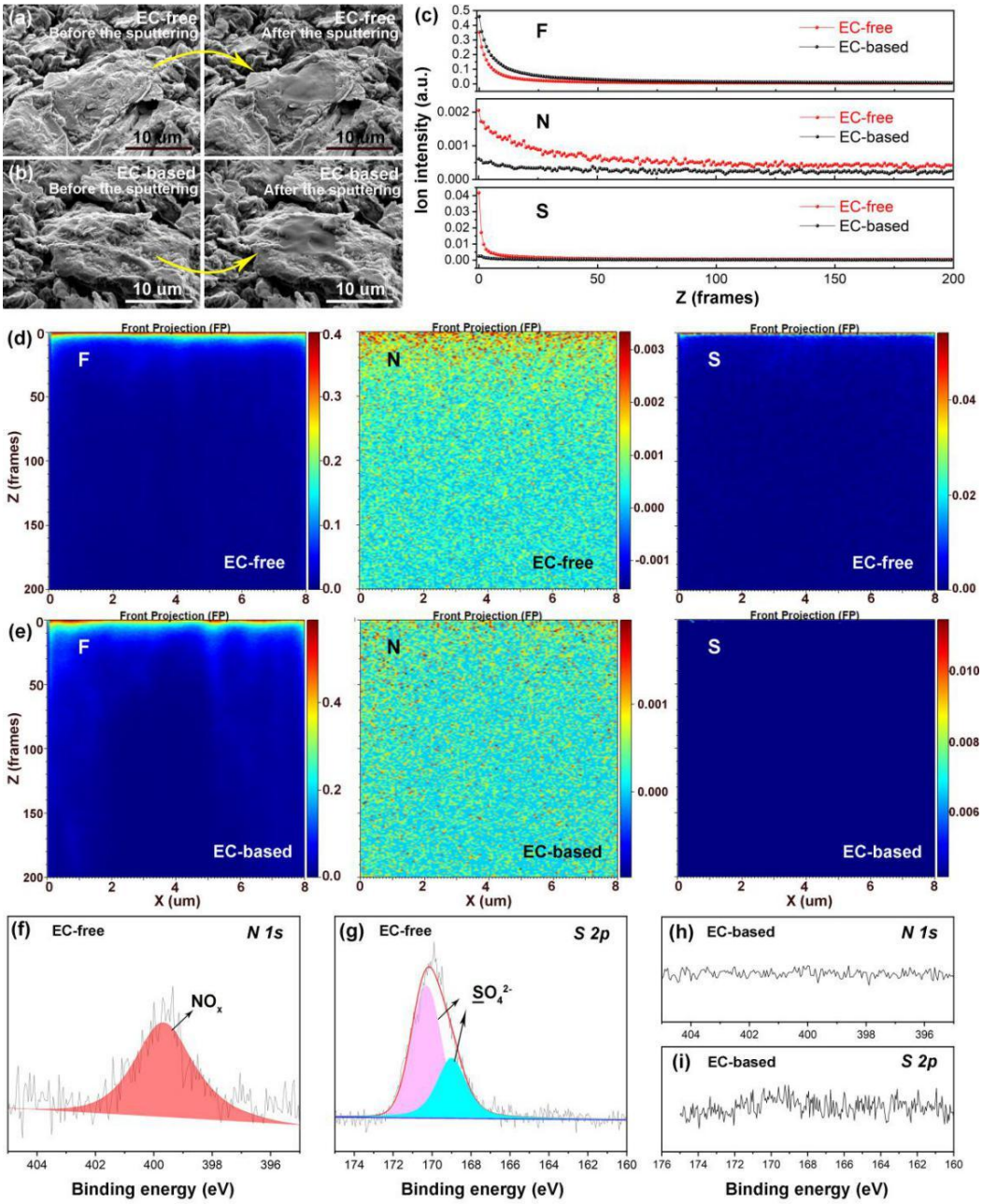

Figure 8. The SEI chemical compositions and depth distribution of the cycled graphite anodes. (a-e) FIB-SEM-ToF-SIMS characterization of the graphite cycled using EC-free electrolytes (a,d) and EC-based electrolytes (b,e). (f-i) XPS characterization of the SEI generated on graphite cycled using EC-free electrolytes (f,g) and EC-based electrolytes (h,i). The N 1s and S 2p spectra.

Conclusions

We have developed an EC-free electrolyte that enables high-safety (TR trigger temperature up to 260.1 °C), long-cycling (~100% capacity retention after 200 cycles), and high-voltage (4.5 V, 82.1 % after 200 cycles) practical Ah-level NMC811|Gr

batteries. Note that the removal of EC solvent greatly benefits the stability of the charged NMC811 with electrolyte. Owing to the synergistic effect of triple-salt, the EC-free electrolyte can form effective CEI to stabilize NMC811 surface under high potential (up to 4.5 V), as well as generate stable interphase to ensure good cycle ability of Gr anode. All these fundamental findings break the traditional electrolyte design framework for Gr-based LIBs, shift the dependence interface layer formation to lithium salt rather than solvent, and extend the conventional knowledge on EC-free electrolyte systems. The work opens up a new direction for both tailoring the electrode materials and developing practical technologies for safe batteries.

Experimental Section

Materials. NMC811|Gr batteries were purchased from LiFun Technology. The mass loading for NMC811 cathodes and graphite anodes were 13.5 and 9.5 mg cm^{-2}, respectively, and 2.4 mL electrolyte was injected into the 1 Ah pouch-type cells. The experimental procedures for the injection, formation, disassembly, and measurements of batteries were similar to that previously reported.[12]

Safety tests. Two cells were connected in parallel and tested for EV-ARC. A K type thermocouple was inserted between the two cells to obtain the internal signals. The experimental procedures for the *operando* HEXRD was similar to that previously reported.[42] NETZSCH DSC 214 Polyma was employed to study the heat flow of charged electrode powders with electrolyte. The sample preparation and testing procedures were consistent with those previously reported.[12]

Characterizations. FIB-SEM-ToF-SIMS combined system was carried out to detect the depth distribution of the cycled electrodes. The Double Cs-Corrected STEM (JEM-ARM300F, Japan) was employed to characterize structural. The surface chemical compositions of the cycled electrodes was analyzed by using XPS and ToF-SIMS 5-100 (ION-TOF GmbH, Germany).

Acknowledgements

This work is supported by Ministry of Science and Technology of China (Grant No.

2019YFE0100200), National Natural Science Foundation of China (Grant No. 52004138 and 52076121), and China Postdoctoral Science Foundation (Grant No. 2021T140361 and 2020M670324). Y. W. acknowledges the support from the Shuimu Tsinghua Scholar Program (No. 2019SM071). Research at the Argonne National Laboratory was funded by the U.S. Department of Energy (DOE), Vehicle Technologies Office. Support from Tien Duong of the U.S. DOE's Office of Vehicle Technologies Program is gratefully acknowledged. Use of the Advanced Photon Source (APS), Office of Science user facilities, was supported by the U. S. Department of Energy, Office of Science, and Office of Basic Energy Sciences, under Contract No. DE-AC02-06CH11357. X.L., G.X. and K.A. acknowledge the support of the U.S. China Clean Energy Research Center (CERC−CVC2).

References

1. M. Armand, J.-M. Tarascon, *Nature* **2008**, *451*, 652.
2. G. W. Crabtree, *Nature* **2015**, *526*, 592.
3. Q. Li, L. Li, P. Wu, N. Xu, L. Wang, M. Li, A. Dai, K. Amine, L. Mai, J. Lu, *Adv. Energy Mater.* **2019**, *9*, 1901153.
4. M. Li, J. Lu, *Science* **2020**, *367*, 979-980.
5. X. Ren, L. Zou, X. Cao, M.H. Engelhard, W. Liu, S.D. Burton, H. Lee, C. Niu, B.E. Matthews, Z. Zhu, C. Wang, B.W. Arey, J. Xiao, J. Liu, J.-G. Zhang, W. Xu, *Joule* **2019**, *3*, 1662.
6. G.-L. Xu, Q. Liu, K.K.S. Lau, Y. Liu, X. Liu, H. Gao, X. Zhou, M. Zhuang, Y. Ren, J. Li, M. Shao, M. Ouyang, F. Pan, Z. Chen, K. Amine, G. Chen, *Nat. Energy* **2019**, *4*, 484.
7. P. Yan, J. Zheng, Z.K. Tang, A. Devaraj, G. Chen, K. Amine, J.G. Zhang, L.M. Liu, C. Wang, *Nat. Nanotechnol.* **2019**, *14*, 602-608.
8. W. Li, E.M. Erickson, A. Manthiram, *Nat. Energy* **2020**, *5*, 26.
9. R. Amine, J. Liu, I. Acznik, T. Sheng, K. Lota, H. Sun, C. Sun, K. Fic, X. Zuo, Y. Ren, D. A. EI-Hady, W. Alshitari, A. S. Al-Bogami, Z. Chen, K. Amine, G.L. Xu, *Adv. Energy Mater.* **2020**, *10*, 2000901.
10. X. Feng, D. Ren, X. He, M. Ouyang, *Joule* **2020**, *4*, 743.
11. Y.K. Sun, Z. Chen, H.J. Noh, D.J. Lee, H.G. Jung, Y. Ren, S. Wang, C.S. Yoon, S.T. Myung, K. Amine, *Nat. Mater.* **2012**, *11*, 942.
12. Y. Wu, X. Feng, X. Liu, X. Wang, D. Ren, L. Wang, M. Yang, Y. Wang, W. Zhang, Y. Li, Y. Zheng, L. Lu, X. Han, G.-L.Xu, Y. Ren, Z. Chen, J. Chen, X. He, K. Amine, M. Ouyang, *Energy Storage Mater.* **2021**, *43*, 248.
13. Y. Li, X. Liu, L.Wang, X., Feng, D. Ren, Y. Wu, G.-L.Xu, X. He, K. Amine, M. Ouyang, *Nano Energy* **2021**, *85*, 105878.
14. K. Liu, W. Liu, Y.C. Qiu, B.A. Kong, Y.M. Sun, Z. Chen, D. Zhuo, D.C. Lin, Y.

Cui, *Sci. Adv.* **2017**, *3*, e1601978.
15. L. Peng, X. Kong, H. Li, X. Wang, C. Shi, T. Hu, Y. Liu, P. Zhang, J. Zhao, *Adv. Funct. Mater.* **2021**, *31*, 2008537.
16. Y.K. Sun, S.T. Myung, B.C. Park, J. Prakash, I. Belharouak, K. Amine, *Nat. Mater.* **2009**, *8*, 320.
17. Y. Ye, L.Y. Chou, Y. Liu, H. Wang, H.K. Lee, W. Huang, J. Wan, K. Liu, G. Zhou, Y. Yang, A. Yang, X. Xiao, X. Gao, D.T. Boyle, H. Chen, W. Zhang, S.C. Kim, Y. Cui, *Nat. Energy* **2020**, *5*, 786.
18. X. Fan, L. Chen, O. Borodin, X. Ji, J. Chen, S. Hou, T. Deng, J. Zheng, C. Yang, S.C. Liou, K. Amine, K. Xu, C. Wang, *Nat. Nanotechnol.* **2018**, *13*, 715.
19. Z. Zeng, V. Murugesan, K.S. Han, X. Jiang, Y. Cao, L. Xiao, X. Ai, H. Yang, J.-G. Zhang, M.L. Sushko, J. Liu, *Nat. Energy* **2018**, *3*, 674.
20. Q. Zheng, Y. Yamada, R. Shang, S. Ko, Y.-Y. Lee, K. Kim, E. Nakamura, A. Yamada, *Nat. Energy* **2020**, *5*, 291.
21. J. Wang, Y. Yamada, K. Sodeyama, E. Watanabe, K. Takada, Y. Tateyama, A. Yamada, *Nat. Energy* **2017**, *3*, 22.
22. Y. Yamada, J. Wang, S. Ko, E. Watanabe, A. Yamada, *Nat. Energy* **2019**, *4*, 269.
23. K. Xu, *Chem. Rev.* **2004**, *104*, 4303.
24. K. Xu, *Chem. Rev.* **2014**, *114*, 11503.
25. J. Xia, R. Petibon, D. Xiong, L. Ma, J.R. Dahn, *J. Power Sources* **2016**, *328*, 124.
26. L. Ma, S.L., Glazier, R. Petibon, J. Xia, J.M. Peters, Q. Liu, J. Allen, R.N.C. Doig, J.R. Dahn, *J. Electrochem. Soc.* **2017**, *164*, A5008.
27. W. Li, A. Dolocan, J. Li, Q. Xie, A. Manthiram, *Adv. Energy Mater.* **2019**, 1901152.
28. S. Klein, S.V. Wickeren, S. Roser, P. Barmann, K. Borzutzki, B. Heidrich, M. Borner, M. Winter, T. Placke, J. Kasnatscheew, *Adv. Energy Mater.* **2021**, 2003738.
29. X. Yu, A. Manthiram, *Energy Environ. Sci.* **2018**, *11*, 527.
30. X. Cao, X. Ren, L. Zou, M.H. Engelhard, W. Huang, Y. Cui, C. Wang, J. Xiao, J. Liu, W. Xu, J.-G. Zhang, *Nat. Energy* **2019**, *4*, 796.
31. J. Chen, X.L. Fan, Q. Li, H.B. Yang, M.R. Khoshi, Y.B. Xu, S. Hwang, L. Chen, C.M. Wang, E. Garfunkel, D. Su, O. Borodin, C.S. Wang, *Nat. Energy* **2020**, *5*, 386.
32. T. Li, X.-Q. Zhang, P. Shi, Q. Zhang, *Joule* **2019**, *3*, 2647.
33. Y. Wu, X. Liu, L. Wang, X. Feng, D. Ren, K. Amine, M. Ouyang, *Energy Storage Mater.* **2021**, *37*, 77.
34. T. Liu, L. Lin, X. Bi, L. Tian, K. Yang, J. Liu, M. Li, Z. Chen, J. Lu, K. Amine, K. Xu, F. Pan, *Nat. Nanotechnol.* **2019**, *14*, 50.
35. H. Maleki Kheimeh Sari, X. Li, *Adv. Energy Mater.* **2019**, *9*, 1901597.
36. W. Zhao, J. Zheng, L. Zou, H. Jia, B. Liu, H. Wang, M.H. Engelhard, C. Wang, W. Xu, Y. Yang, J.-G. Zhang, *Adv. Energy Mater*. **2018**, *8*, 1800297.
37. X. Feng, M. Ouyang, X. Liu, L. Lu, Y. Xia, X. He, *Energy Storage Mater.* **2018**, *10*, 246.
38. X. Feng, S. Zheng, D. Ren, X. He, L. Wang, H. Cui, X.Liu, C. Jin, F. Zhang, C. Xu, *Appl. Energy* **2019**, *246*, 53-64.
39. D. Ren, H. Hsu, R. Li, X. Feng, D. Guo, Y. Wang, M. Ouyang, *eTransportation*

2019, *2*, 100034.
40. J. Hou, L. Lu, L. Wang, A. Ohma, Y. Nitta, M. Ouyang, *Nat. Commun.* **2020**, *11*, 5100.
41. Y. Li, X. Liu, D. Ren, H. Hsu, G. Xu, X. He, K. Amine, M. Ouyang, *Nano Energy* **2020**, *71*, 104643.
42. X. Liu, G.-L. Xu, L. Yin, I. Hwang, Y. Li, Y. Ren, C.-J. Sun, Z. Chen, M. Ouyang, K. Amine, *J. Am. Chem. Soc.* **2020**, *142*, 19745.
43. S. M. Bak, E. Hu, Y. Zhou, X. Yu, S. D. Senanayake, S. J. Cho, K. B. Kim, K. Y. Chung, X. Q. Yang, K. W. Nam, *ACS Appl. Mater. Interfaces* **2014**, *6*, 22594.
44. X. Ren, L. Zou, S. Jiao, D. Mei, M.H. Engelhard, Q. Li, H. Lee, C. Niu, B.D. Adams, C. Wang, J. Liu, J.-G. Zhang, W. Xu, *ACS Energy Lett.* **2019**, *4*, 896-902.
45. W. Liu, J. Li, W. Li, H. Xu, C. Zhang, X. Qiu, *Nat. Commun.* **2020**, *11*, 3629.